# REPORT DOCUMENTATION PAGE

*Form Approved*
*OMB No. 0704-0188*

Public reporting burden for this collection of information is estimated to average 1 hour per response, including the time for reviewing instructions, searching existing data sources, gathering and maintaining the data needed, and completing and reviewing this collection of information. Send comments regarding this burden estimate or any other aspect of this collection of information, including suggestions for reducing this burden to Department of Defense, Washington Headquarters Services, Directorate for Information Operations and Reports (0704-0188), 1215 Jefferson Davis Highway, Suite 1204, Arlington, VA  22202-4302.  Respondents should be aware that notwithstanding any other provision of law, no person shall be subject to any penalty for failing to comply with a collection of information if it does not display a currently valid OMB control number. **PLEASE DO NOT RETURN YOUR FORM TO THE ABOVE ADDRESS.**

| 1. REPORT DATE *(DD-MM-YYYY)*<br>20-08-2007 | 2. TYPE REPORT<br>Journal Article | 3. DATES COVERED *(From - To)*<br>01 Dec 06 |
|---|---|---|

**4. TITLE AND SUBTITLE**

Statistical analysis of measured polarimetric clutter data at different range resolutions

**5a. CONTRACT NUMBER**

**5b. GRANT NUMBER**

**5c. PROGRAM ELEMENT NUMBER**
61102F

**6. AUTHOR(S)**

*Maria Greco, *Fulvio Gini, Muralidhar Rangaswamy

**5d. PROJECT NUMBER**
2311

**5e. TASK NUMBER**
HE

**5f. WORK UNIT NUMBER**
02

**7. PERFORMING ORGANIZATION NAME(S) AND ADDRESS(ES)**

AFRL/SNHE
80 Scott Drive
Hanscom AFB MA 01731

*Dipartimento di Ingegneria dell'Informazione,
Université di Pisa
via G Caruso
Pisa 14-1-57122, Italia

**8. PERFORMING ORGANIZATION REPORT**

**9. SPONSORING / MONITORING AGENCY NAME(S) AND ADDRESS(ES)**
Electromagnetics Technology Division          SC: 437490
Sensors Directorate
Air Force Research Laboratory
80 Scott Drive
Hanscom AFB MA 01731-2909

**10. SPONSOR/MONITOR'S ACRONYM(S)**

AFRL-SN-HS

**11. SPONSOR/MONITOR'S REPORT NUMBER(S)**
AFRL-SN-HS-TP-2007-0008

**12. DISTRIBUTION / AVAILABILITY STATEMENT**
DISTRIBUTION A.  Approved for public release; distribution unlimited.

**13. SUPPLEMENTARY NOTES**
Supported by European Office of Aerospace Research and Development (EOARD) under contract number FA8655-04-1-3059 for AFRL/SNHE, IN-HOUSE work unit 2311HE02. Published in IEE Proc.-Radar Sonar Navig., Vol. 153, No. 6, December 2006. Cleared for Public Release by ESC/PA: ESC 06-0396 dtd 4 Apr 06

**14. ABSTRACT**
This paper deals with the statistical modelling of radar backscattering from sea surface at low-grazing angles in high resolution radar systems. High-Resolution polarimetric data at different range resolutions (60, 30, 15, 9 and 3m) are analysed to highlight the differences in clutter statistical behaviour due to changes of resolution and/or polarisation. The clutter data were recorded by the IPIX radar of McMaster University in Grimsby. Ontario Canada..

**15. SUBJECT TERMS**
Statistical analysis lake surface scattering, high-resolution polarimetric data characterization, small-scale Bragg resonant waves, lake clutter non-stationarity

| 16. SECURITY CLASSIFICATION OF: | | | 17.LIMITATION OF ABSTRACT | 18.NUMBER OF PAGES | 19a. NAME OF RESPONSIBLE PERSON<br>Muralidhar Rangaswamy |
|---|---|---|---|---|---|
| **a. REPORT**<br>Unclassified | **b. ABSTRACT**<br>Unclassified | **c. THIS PAGE**<br>Unclassified | UU | 11 | **19b. TELEPHONE NUMBER** *(include area code)*<br>N/A |

**Standard Form 298 (Rev. 8-98)**
**Prescribed by ANSI Std. Z39.18**

# Statistical analysis of measured polarimetric clutter data at different range resolutions

M. Greco, F. Gini and M. Rangaswamy

**Abstract:** This paper deals with the statistical modelling of radar backscattering from sea surface at low-grazing angles in high resolution radar systems. High-resolution polarimetric data at different range resolutions (60, 30, 15, 9 and 3 m) are analysed to highlight the differences in clutter statistical behaviour due to changes of resolution and/or polarisation. The clutter data were recorded by the IPIX radar of McMaster University in Grimsby, Ontario, Canada.

## 1 Radar and data description

The clutter data processed in this paper were collected using the McMaster University IPIX radar. IPIX is an X-band search radar, capable of dual-polarised and frequency-agile operation [1]. The characteristic features of the IPIX radar are summarised in Table 1.

The radar site is located to the east of 'Place Polonaise' at Grimsby, Ontario (latitude 43.2114 N, longitude 79.5985 W), looking at lake Ontario from a height of 20 m. The data of the OHGR database are stored in 222 files, as 10 bit integers. There are like-polarisations, HH and VV (Lpol), and cross-polarisations, HV and VH (Xpol), with coherent processing being received, leading to a quadruplet of I and Q values for Lpol and Xpol.

We analysed many files with different range resolutions and recorded on different days. In this work, we summarise the results relating to only five files, containing more than 8 million samples, recorded on 4 February 1998 at about 22:30 hours (local time). They are representative of most of the results obtained from all the processed data. Unfortunately, there is no available information about the wind and wave observations for these data sets. The relevant parameters are summarised in Fig. 1 and Table 2.

It is important to observe that in each file the range resolution is different and that at 30 m, the illuminated zone is different with respect to that illuminated at 60, 15, 9 and 3 m range resolution. These files were chosen to highlight the differences due to the change in the resolution.

The IPIX receiver has two operational modes depending upon the selected RF pulse width (PW). When the system is operating with PW ≥ 200 ns, a 5 MHz filter is used to limit the receiver bandwidth to ~5 MHz. When at PW < 200 ns, this filter is bypassed, so the bandwidth of the receiver is ~50 MHz to match the minimum 20 ns PW. Therefore for data collected with PW < 200 ns, the

noise floor is about 10 dB higher than for data collected with PW ≥ 200 ns [2].

## 2 Statistical analysis

### 2.1 Statistical models of clutter amplitude

Many distributions have been proposed in the literature to model the amplitude probability density function (PDF) of high resolution non-Gaussian clutter ([3–14], and references therein). Here, we compare the empirical PDF with log-normal (LN), Weibull (W), K and generalised K (GK) PDFs. The analytical expressions for these PDFs and their moments $m_R(n) = E\{r^n\}$ are reported below [7], where $r = |z|$ denotes the clutter amplitude and $z$ its complex envelope.

*LN model*

$$\text{PDF} \quad p_R(r) = \frac{1}{r\sqrt{2\pi\sigma^2}} \exp\left(-\frac{1}{2\sigma^2}\left[(\ln r - \ln \delta)^2\right]\right)u(r) \tag{1}$$

$$\text{Moments} \quad m_R(n) = \delta^n \exp\frac{n^2\sigma^2}{2} \tag{2}$$

where $\sigma$ is the shape parameter, $\delta$ the scale parameter and $u(r)$ the unit step function.

*Weibull model (W)*

$$\text{PDF} \quad p_R(r) = \frac{c}{b^c}r^{c-1}\exp\left[-\left(\frac{r}{b}\right)^c\right]u(r) \tag{3}$$

$$\text{Moments} \quad m_R(n) = b^n\Gamma\left(\frac{n}{c}+1\right) \tag{4}$$

where $c$ is the shape parameter and $b$ the scale parameter. The Rayleigh PDF is a particular case of the Weibull PDF for $c = 2$.

*K-model (K)*

$$\text{PDF} \quad p_R(r) = \frac{\sqrt{2\nu/\mu}}{2^{\nu-1}\Gamma(\nu)}\left(\sqrt{\frac{2\nu}{\mu}}\,r\right)^\nu K_{\nu-1}\left(\sqrt{\frac{2\nu}{\mu}}\,r\right)u(r) \tag{5}$$

$$\text{Moments} \quad m_R(n) = \left(\frac{2\mu}{\nu}\right)^{n/2}\frac{\Gamma(\nu+n/2)\Gamma(1+n/2)}{\Gamma(\nu)} \tag{6}$$

## Table 1: Characteristics of the IPIX radar

| Transmitter | Receiver | Parabolic dish antenna |
|---|---|---|
| TWT peak power: 8 KW | Two receivers | Diameter: 2.4 m |
| Dual frequency simultaneous transmission: 8.9–9.4 GHz | Outputs: linear, I and Q | Pencil beam width (azimuth resolution): 1.1 |
| H-V polarisation, agile | Receiving polarisations: H-V | Antenna gain: 45.7 dB |
| PW: 20–5000 ns (real) 5000 ns (expanded) 32 ns (compressed) | Data acquisition: sample rate from 0 to 50 MHz outputs: linear, I and Q | Cross-polarisation isolation: 30 dB |
| PRF: from 0 to 20 KHz | Quantisation: 10 bit up to 16 bit effective with H/W decimation | Double polarisation with central feeder |

| Name of the data set | 19980204_223753 ANTSTEP | 19980204_220849 ANTSTEP | 19980204_223220 ANTSTEP | 19980204_224024_ANTSTEP | 19980204_223506 ANTSTEP |
|---|---|---|---|---|---|
| Date, time of acquisition | 02/04/1998 22:37:53 | 02/04/1998 22:08:49 | 02/04/1998 22:32:20 | 02/04/1998 22:40:24 | 02/04/1998 22:35:06 |
| No. of range cells | 28 | 28 | 28 | 28 | 27 |
| Start range | 3201 m | 3201 m | 3201 m | 3201 m | 3321 m |
| Range resolution | 60 m | 30 m | 15 m | 9 m | 3 m |
| PW | 400 ns | 200 ns | 100 ns | 60 ns | 20 ns |
| Total no. of sweep | 60 000 | 60 000 | 60 000 | 60 000 | 60 000 |
| Sample for cell | 60 000 sampled at 60 m | 60 000 sampled at 30 m | 60 000 sampled at 15 m | 60 000 sampled at 9 m | 60 000 sampled at 3 m |
| PRF | 1 KHz | 1 KHz | 1 KHz | 1 KHz | 1 KHz |
| Frequency RF | 9.39 GHz | 9.39 GHz | 9.39 GHz | 9.39 GHz | 9.39 GHz |
| Radar and wave geometry | | | | | |

**Fig. 1** *Characteristics of the analysed files*

where $\Gamma(\cdot)$ is the gamma function, $K_{\nu-1}(\cdot)$ the modified Bessel function of the third kind of order $\nu - 1$, $\nu$ the shape parameter and $\mu$ the scale parameter.

*GK model with log-normal texture*

$$\text{PDF} \quad p_R(r) = \frac{r}{\sqrt{2\pi\sigma^2}}\int_0^\infty \frac{2}{\tau^2}\exp\left[\frac{r^2}{\tau} - \frac{1}{2\sigma^2}\left[\ln\left(\frac{\tau}{2m}\right)\right]^2\right]d\tau \tag{7}$$

$$\text{Moments} \quad m_R(n) = (2m)^{n/2}\Gamma\left(1 + \frac{n}{2}\right)\exp\left(\frac{n^2\sigma^2}{8}\right) \tag{8}$$

where $\sigma$ is the shape parameter and $m$ the scale parameter.

*GK model with generalised gamma texture*

$$\text{PDF} \quad p_R(r) = \frac{2br}{\Gamma(\nu)}\left(\frac{\nu}{\mu}\right)\int_0^\infty \tau^{\nu b - 2}\exp\left[\frac{r^2}{\tau} - \left(\frac{\nu}{\mu}\tau\right)^b\right]d\tau \tag{9}$$

$$\text{Moments} \quad m_R(n) = \left(\frac{\mu}{\nu}\right)^{n/2}\Gamma\frac{(\nu + n/2b)\Gamma(1 + n/2)}{\Gamma(\nu)} \tag{10}$$

Apart from LN model, the other PDFs considered here belong to the so-called compound-Gaussian family. Specifically, they arise from the product of two random variables: the texture and the speckle. According to this model, the samples of the complex envelope of the sea clutter process can be represented as

$$z(i) = \sqrt{\tau(i)}x(i), \quad i = 1, 2, \dots, N_S \tag{11}$$

## Table 2: Estimated parameters, 60 m

| Cell | W | | LN | | K | | LNT | | GK | | |
|---|---|---|---|---|---|---|---|---|---|---|---|
| | $\hat{c}$ | $\hat{b}$ | $\hat{\sigma}$ | $\hat{\delta}$ | $\hat{\nu}$ | $\hat{\mu}$ | $\hat{\sigma}^2$ | $\hat{m}$ | $\hat{\nu}$ | $\hat{\mu}$ | $\hat{b}$ |
| VV-15th | 1.391 | 0.014 | 0.652 | 0.010 | 1.331 | $1.268 \times 10^4$ | 0.736 | $8.760 \times 10^5$ | 5.500 | $2.798 \times 10^5$ | 0.461 |
| Mean | 1.293 | 0.021 | 0.695 | 0.015 | 1.119 | $4.718 \times 10^4$ | 1.020 | $2.694 \times 10^4$ | 20.57 | $2.604 \times 10^4$ | 0.427 |
| HH-15th | 1.324 | 0.016 | 0.677 | 0.012 | 1.122 | $1.671 \times 10^4$ | 0.867 | $1.083 \times 10^4$ | 6.010 | $1.888 \times 10^5$ | 0.408 |
| Mean | 1.226 | 0.022 | 0.722 | 0.016 | 0.927 | $4.162 \times 10^4$ | 1.133 | $2.210 \times 10^4$ | 15.55 | $2.758 \times 10^4$ | 0.428 |
| HV-15th | 1.386 | 0.014 | 0.654 | 0.011 | 1.316 | $1.321 \times 10^4$ | 0.744 | $9.106 \times 10^4$ | 5.341 | $3.123 \times 10^5$ | 0.465 |
| Mean | 1.292 | 0.021 | 0.695 | 0.016 | 1.117 | $4.179 \times 10^4$ | 0.980 | $2.330 \times 10^4$ | 19.70 | $2.734 \times 10^4$ | 0.430 |

LNT, LN texture

where $N_s$ denotes the number of samples. The term $x(i) = x_I(i) + jx_Q(i)$ represents a stationary complex-Gaussian process, usually called speckle, which accounts for local backscattering; $x_I(i)$ and $x_Q(i)$ are the in-phase and quadrature components of the speckle complex envelope $x(i)$. They satisfy the property $E\{x_I(i)\} = E\{x_Q(i)\} = 0$, and $E\{x_I^2(i)\} = E\{x_Q^2(i)\} = 1/2$, so that $E\{|x(i)|^2\} = 1$, that is, the speckle complex samples have unit power. The factor $\tau(i)$ is a non-negative real random process, usually called texture, that models the local clutter power.

Given the speckle and texture PDFs, it is possible to obtain the amplitude PDF as follows

$$z(i) = \sqrt{\tau(i)}x(i) \Rightarrow r(i) = |z(i)| = \sqrt{\tau(i)}|x(i)| \quad (12)$$

$$p_R(r) = \int_{-\infty}^{+\infty} p_R(r|\tau)p_\tau(\tau)\,d\tau \quad (13)$$
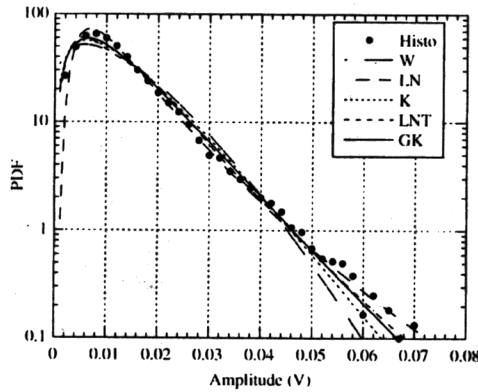


**Fig. 2** *Clutter amplitude PDF, VV polarisation, 15th range cell, 60 m*
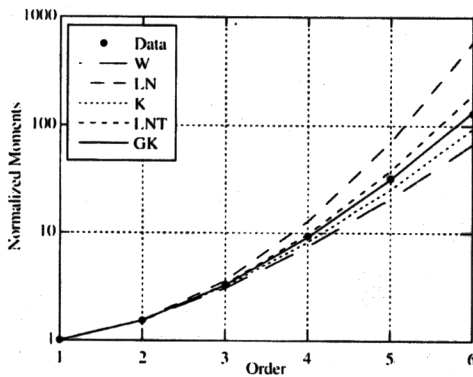


**Fig. 3** *Normalised clutter moments, VV polarisation, 15th range cell, 60 m*

The parameters of the theoretical PDFs are estimated by the classical method of moments (MoM) [15], which consists of equating the first- and second-order experimental moments with the corresponding theoretical moments. The estimated moments are given by

$$\hat{m}_R(n) = \frac{1}{N_S} \sum_{i=1}^{N_S} |z(i)|^n \quad (14)$$

We processed $N_s = 60\,000$ samples for each range cell. As concerning the parameters of the GK-PDF, we encountered a numerical problem with the above approach. Therefore in this case, we used a number of empirical moments greater than the number of unknowns. As a result, the parameters $\nu$ and $b$ were estimated as

$$(\hat{\nu}, \hat{b}) = \arg\min_{(\nu,b)} J(\nu, b) = \arg\min_{(\nu,b)} \sum_{n=2}^{5} \left| \frac{\hat{m}_R(n) - m_R(n)}{m_R(n)} \right|^2 \quad (15)$$

The absolute minimum of the functional in (15) was found by two successive two-dimensional grid searches, as described in Farina *et al.* [7]. Once $\nu$ and $b$ have been estimated, $\hat{\mu}$ is obtained from an estimate, $\hat{m}_R(1)$, of the first-order moment.

### 2.2 Range resolutions of 60, 30 and 15 m

The results of the statistical analysis by means of histograms and moments calculation reveal that the GK-PDF yields a good-fit for both like- and cross-polarised data and for all the three resolutions. Therefore the analysed clutter process can be accurately modelled by a compound-Gaussian process with GK-PDF, provided that the size of the range resolution cell is $\geq 15$ m (note that the Gaussian model is a particular case of the GK model).

In Figs. 2 and 3, we report the histogram and the moments for the 15th range cell, VV data, 60 m range resolution. The numerical results for the other range cells and the two other range resolutions are very similar. Therefore they are not reported here.

In Table 2, we report the mean values of the parameters estimated for each theoretical PDF. The results show that, for a resolution of 60 m, on average, the HH component is spikier ($\bar{c} = 1.226$) than both VV ($\bar{c} = 1.293$) and VH ($\bar{c} = 1.292$) components. (Results for different polarisations have been compared with respect to the mean value ($\bar{c}$) of the estimates $\hat{c}$ of parameter $c$ of the Weibull distribution, because the meaning of this parameter is quite easy to understand.) Moreover, the parameters estimated when the range resolution is 30 m (Table 3) show that the data are spikier at 30 m range resolution than at 60 m; this was found for all polarisations. Moreover, we found that VV data ($\bar{c} = 1.094$) and VH data ($\bar{c} = 1.093$) are spikier than HH data ($\bar{c} = 1.218$).

**Table 3:** Estimated parameters, 30 m

| Mean | W | | LN | | K | | LNT | | GK | | |
|------|------|------|------|------|------|------|------|------|------|------|------|
| | $\hat{c}$ | $\hat{b}$ | $\hat{\sigma}$ | $\hat{\delta}$ | $\hat{\nu}$ | $\hat{\mu}$ | $\hat{\sigma}^2$ | $\hat{m}$ | $\hat{\nu}$ | $\hat{\mu}$ | $\hat{b}$ |
| VV | 1.094 | 0.015 | 0.791 | 0.011 | 0.681 | $2.331 \times 10^{4}$ | 1.573 | $1.033 \times 10^{-4}$ | 12.80 | $1.946 \times 10^{4}$ | 0.436 |
| HH | 1.218 | 0.005 | 0.729 | 0.003 | 0.944 | $1.701 \times 10^{5}$ | 1.182 | $8.966 \times 10^{6}$ | 29.77 | $8.766 \times 10^{6}$ | 0.335 |
| HV | 1.093 | 0.016 | 0.792 | 0.011 | 0.678 | $2.468 \times 10^{4}$ | 1.577 | $1.094 \times 10^{4}$ | 12.28 | $2.061 \times 10^{4}$ | 0.437 |

LNT, LN texture

**Table 4: Estimated parameters, 15 m**

| Mean | W | | LN | | K | | LNT | | GK | | |
|---|---|---|---|---|---|---|---|---|---|---|---|
| | $\hat{c}$ | $\hat{b}$ | $\hat{\sigma}$ | $\hat{\delta}$ | $\hat{\nu}$ | $\hat{\mu}$ | $\hat{\sigma}^2$ | $\hat{m}$ | $\hat{\nu}$ | $\hat{\mu}$ | $\hat{b}$ |
| VV | 0.933 | 0.029 | 0.895 | 0.021 | 0.466 | 0.001 | 2.309 | $3.450 \times 10^{-4}$ | 3.602 | 0.001 | 0.459 |
| HH | 0.874 | 0.024 | 0.935 | 0.017 | 0.383 | $9.364 \times 10^{-4}$ | 2.592 | $2.305 \times 10^{-4}$ | 3.281 | $9.979 \times 10^{-4}$ | 0.474 |
| HV | 1.018 | 0.011 | 0.840 | 0.008 | 0.592 | $1.424 \times 10^{-4}$ | 1.905 | $5.198 \times 10^{-5}$ | 3.845 | $1.078 \times 10^{-4}$ | 0.467 |

LNT, LN texture
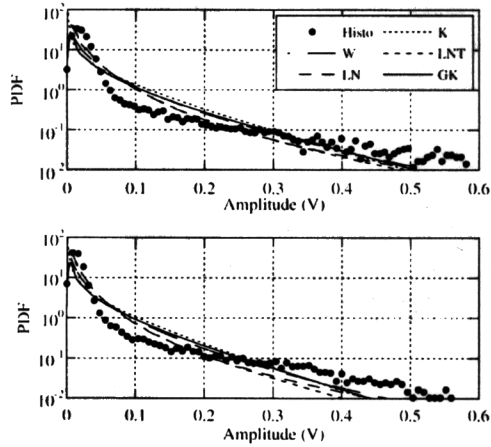


**Fig. 4** *Clutter amplitude PDF, VV and HH polarisations, fifth range cell, 9 m*

For the range resolution of 15 m and for co-polarisations, we observed the presence of some more heavy-tailed behaviour (e.g. in the 7th and 24th cells of the file 19980204_223220), but generally the GK model provides a good-fit to the data. The values of the estimated parameters confirm that the clutter becomes spikier when range resolution increases (i.e. the size of the resolution cell decreases). We also noticed that on an average HH data are spikier ($\bar{c} = 0.874$) than VV data ($\bar{c} = 0.933$) and VH data ($\bar{c} = 1.018$); the same happened for the 60 m resolution data (Table 4).

### 2.3 Range resolutions of 9 and 3 m

Examining the histograms obtained by analysing the file at a resolution of 9 m, we found that many cells of co-polarised data exhibit heavy tails and none of the proposed models yields a good-fit to the data. One of these cells is the fifth, plotted in Fig. 4 for VV and HH data. On the contrary, we observed that for cross-polarisations, the clutter process can still be accurately modelled by a compound-Gaussian process with GK-PDF. Again, the values of the estimated parameters show that HH data have the spikiest behaviour (HH: $\bar{c} = 0.991$, VV: $\bar{c} = 1.099$, VH: $\bar{c} = 1.175$) (Table 5). The same was found for both 60 and 15 m range resolution data.

The results obtained for co-polarisations at a range resolution of 3 m do not show significant differences with respect to the results obtained at 9 m. Conversely, the analysis for VH polarisation presents some difference. There are cells showing histograms with tails longer than the average length recorded at lower resolutions; in this case, the compound model cannot be used to model clutter data.

The estimates of the parameters are reported in Table 6. The results show again that HH data ($\bar{c} = 1.307$) are spikier than VV ($\bar{c} = 1.542$) data. With respect to the other resolutions, estimated values of $\bar{c}$ are slightly higher, probably because of thermal noise effect.

**Table 5: Estimated parameters, 9 m**

| Cell | W | | LN | | K | | LNT | | GK | | |
|---|---|---|---|---|---|---|---|---|---|---|---|
| | $\hat{c}$ | $\hat{b}$ | $\hat{\sigma}$ | $\hat{\delta}$ | $\hat{\nu}$ | $\hat{\mu}$ | $\hat{\sigma}^2$ | $\hat{m}$ | $\hat{\nu}$ | $\hat{\mu}$ | $\hat{b}$ |
| VV-fifth | 0.585 | 0.021 | 1.207 | 0.016 | 0.129 | 0.002 | 4.861 | $2.032 \times 10^{-4}$ | 0.216 | 0.005 | 0.638 |
| Mean | 1.099 | 0.028 | 0.806 | 0.020 | 0.781 | $8.523 \times 10^{-4}$ | 1.732 | $3.261 \times 10^{-4}$ | 35.69 | $4.025 \times 10^{-4}$ | 0.227 |
| HH-fifth | 0.548 | 0.015 | 1.261 | 0.011 | 0.108 | 0.002 | 5.395 | $1.041 \times 10^{-4}$ | 0.147 | 0.003 | 0.727 |
| Mean | 0.991 | 0.021 | 0.868 | 0.015 | 0.564 | $5.852 \times 10^{-4}$ | 2.150 | $1.825 \times 10^{-4}$ | 22.59 | $3.777 \times 10^{-4}$ | 0.278 |
| HV-fifth | 0.626 | 0.007 | 1.153 | 0.005 | 0.154 | $2.085 \times 10^{-4}$ | 4.352 | $2.367 \times 10^{-5}$ | 0.459 | $2.680 \times 10^{-4}$ | 0.478 |
| Mean | 1.175 | 0.009 | 0.765 | 0.007 | 0.957 | $8.157 \times 10^{-5}$ | 1.461 | $3.578 \times 10^{-5}$ | 33.01 | $3.832 \times 10^{-5}$ | 0.259 |

LNT, LN texture

**Table 6: Estimated parameters, 3 m**

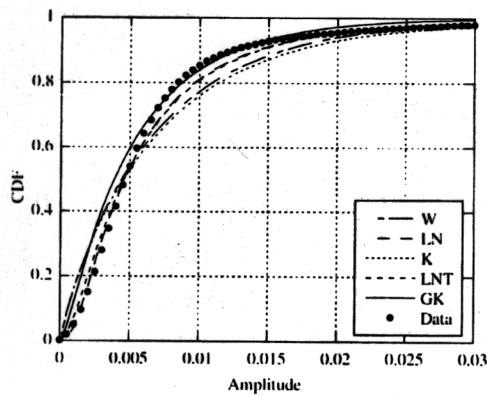| Mean | W | | LN | | K | | LNT | | GK | | |
|---|---|---|---|---|---|---|---|---|---|---|---|
| | $\hat{c}$ | $\hat{b}$ | $\hat{\sigma}$ | $\hat{\delta}$ | $\hat{\nu}$ | $\hat{\mu}$ | $\hat{\sigma}^2$ | $\hat{m}$ | $\hat{\nu}$ | $\hat{\mu}$ | $\hat{b}$ |
| VV | 1.417 | 0.038 | 0.668 | 0.028 | 2.621 | 0.001 | 0.889 | $6.470 \times 10^{-4}$ | 59.17 | $1.997 \times 10^{6}$ | 0.148 |
| HH | 1.307 | 0.027 | 0.709 | 0.019 | 1.588 | $5.580 \times 10^{-4}$ | 1.118 | $3.071 \times 10^{-4}$ | 54.83 | $2.672 \times 10^{6}$ | 0.139 |
| HV | 1.542 | 0.009 | 0.619 | 0.006 | 3.960 | $4.550 \times 10^{-5}$ | 0.608 | $3.284 \times 10^{-5}$ | 63.98 | $2.01 \times 10^{10}$ | 0.148 |

LNT, LN texture

**Fig. 5** *Clutter amplitude distributions, VV data, seventh range cell, 15 m*

**Table 7: Probability of Type I error, KS test, seventh range cell, VV data, 9 m**

| W | LN | K | GK | LNT |
|-----|-----|-----|-----|-----|
| 52% | 0% | 51% | 33% | 0% |

LNT, LN texture

The statistical analysis of clutter amplitude was completed by applying the Kolmogorov–Smirnoff (KS) goodness-of-fit test. This test is largely used to determine which distribution provides the best-fit to the data. Unfortunately, in some cases, it was not useful in distinguishing between different long-tailed models, because it places an equal importance on all regions in the probability space. Therefore in the heaviest part of the PDF, that is, the most affecting the results of the test is the 'bell' area or the body of the PDFs, many of the tested PDFs are very similar. The test is characterised by the probability of Type I error. The Type I error is the probability of observing under $H_0$ a sample outcome at least as extreme as the one observed and hence provides the smallest level at which the observed sample statistic is significant [16].

For resolutions of 60 and 30 m, for all the tested models, we obtained a probability of Type I in the range of 1–5%. Some differences were found at higher resolutions. In Fig. 5, we show the empirical and theoretical distributions for a heavy-tailed range cell, the seventh cell for VV data at a resolution of 15 m. The results of the KS test for this cell are summarised in Table 7. For resolution higher than 30 m, the KS test provides the highest probability of Type I error particularly for the LN distribution.

## 3 Cumulant domain analysis

To perform additional analysis of the compound-Gaussian model and to investigate whether the deviation from the theoretical models in the highest two resolutions, that is, 9 and 3 m, may be due to the presence of non-negligible thermal noise, we applied the theory of cumulants [17]. It is widely known in the literature that cumulants of order greater than two for a Gaussian process are identically zero [17, 18]. Thus, if we consider the clutter process $z(i) = y(i) + v(i)$, where $v(i)$ is a Gaussian process and

$y(i)$ is a non-Gaussian process, independent of $v(i)$, we have

$$c_k^z(l_1, \ldots, l_{k-1}) = c_k^y(l_1, \ldots, l_{k-1}) + c_k^v(l_1, \ldots, l_{k-1})$$
$$= c_k^y(l_1, \ldots, l_{k-1}), \quad \text{for } k > 2 \qquad (16)$$

so the cumulants of $y(i)$ can be derived from the cumulants of $z(i)$. In our case, the in-phase (I) and quadrature (Q) components of the thermal noise are zero-mean-Gaussian processes, then only non-Gaussian clutter contributes to the third-, fourth- and fifth-order cumulants of the observed complex data.

We estimated from the data the second, third and fifth-order cumulants at zero lags, that is, for $l_1 = l_2 = l_{k-1} = 0$. Then, the cumulants are normalised with respect to the second order cumulant as follows

$$\mu_k = \frac{c_k^I(0, 0, \ldots, 0)}{(c_2^I(0))^{k/2}} = \frac{c_k^Q(0, 0, \ldots, 0)}{(c_2^Q(0))^{k/2}} \qquad (17)$$

where superscripts I and Q refer to the in-phase and quadrature components, that is, the real and imaginary parts of the complex data. We compared the estimates with the (normalised) theoretical cumulants of the compound-Gaussian model calculated at zero lags. All the theoretical cumulants of odd order calculated at the origin are equal to zero.

In Figs. 6 and 7, we show the normalised cumulants $\mu_3$ and $\mu_5$ against the second-order cumulant for the
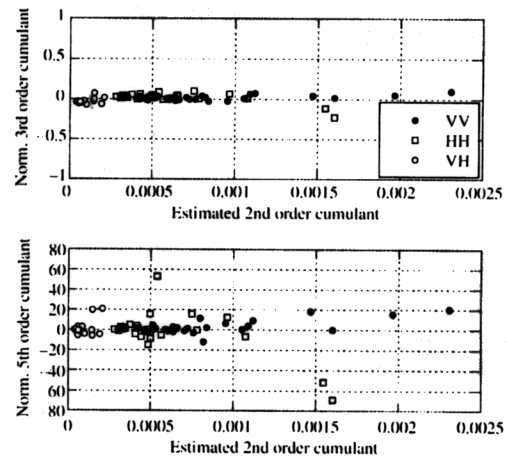


**Fig. 6** *Normalised third- and fifth-order cumulants against second-order cumulant, 9 m*
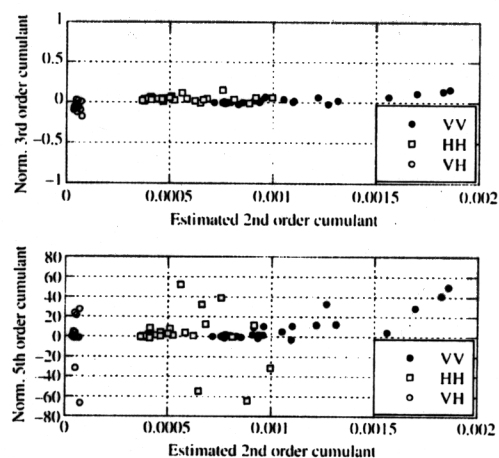


**Fig. 7** *Normalised third- and fifth-order cumulants against second-order cumulant, 3 m*

resolutions of 9 and 3 m, respectively. The results show that at a range resolution of 9 m, the compound-Gaussian model is still accurate. Moreover, it can be adopted to model the clutter process in most cells also for VH polarisation. In fact, for VH data $\mu_3$ and $\mu_5$ are close to zero. Conversely, the fifth-order cumulant shows a large deviation from zero in most cells, for both HH and VV polarisations. At a range resolution of 3 m, for most cells and all polarisations, the estimated cumulants deviate significantly from zero. This is an indication that the thermal noise is not the cause of the deviation from the compound-Gaussian family.

## 4 Correlation analysis and power spectrum estimation

The compound-Gaussian clutter model assumes the presence of two components, speckle and texture, with very different correlation times (some milliseconds for the first component and some seconds for the second one). If the two components are statistically independent, the overall autocorrelation function is the product of the autocorrelation functions of the two components [7, 19]

$$R_Z(m) = E\{z(i)z^*(i+m)\} = R_{\sqrt{\tau}}(m)R_X(m)$$

$$= 2R_{\sqrt{\tau}}(m)\left(R_{X_I}(m) + jR_{X_I X_Q}(m)\right) \quad (18)$$

where we exploited the fact that if the speckle is a complex-valued stationary circular process, then $R_{X_I}(m) = R_{X_Q}(m)$. In practice, the decorrelation time of the signal $z(i)$, called coherent signal, is equal to that of the faster component [7].

### 4.1 Estimation of the speckle autocorrelation and cross-correlation sequences

As the texture can be considered constant over short time intervals, we can estimate the speckle autocorrelation functions $R_{X_I}(m)$ and $R_{X_I X_Q}(m)$ by using coherent signal samples from such short intervals with or without overlapping

$$\hat{R}_{X_I}(m) = \frac{1}{N_b}\left[\sum_{k=1}^{N_b}\frac{1}{2N\hat{\tau}_k}\text{Re}\left\{\sum_{i=0}^{N-1-m}z_k(i)z_k^*(i+m)\right\}\right] \quad (19)$$

$$\hat{R}_{X_I X_Q}(m) = \frac{1}{N_b}\left[\sum_{k=1}^{N_b}\frac{1}{2N\hat{\tau}_k}\text{Im}\left\{\sum_{i=0}^{N-1-m}z_k(i)z_k^*(i+m)\right\}\right] \quad (20)$$

where $N_b$ is the number of data bursts and $\hat{\tau}_k$ the estimated value of the texture in the $k$th burst

$$\hat{\tau}_k = \frac{1}{N}\sum_{i=0}^{N-1}|z_k(i)|^2 \quad (21)$$

where $z_k(i) = z((k-1)N+i)$. We used three different values of $N$: 64, 128 and 256, with an overlap between bursts of 50%. We did not find apparent differences in the estimation for $N = 64$, 128 and 256, so we show here only the results for $N = 128$.

Figs. 8 and 9 show two plots of the real and the imaginary parts of the speckle autocorrelation function. The whole results provide a clear indication that for all resolutions and all polarisations, the speckle correlation time is about 10 ms long and the behaviour is oscillatory, as in Figs. 8 and 9 for 60 and 3 m, respectively.
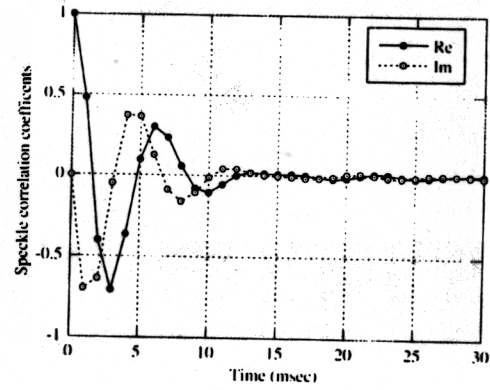
**Fig. 8** *Speckle correlation coefficients, HH polarisation, first cell, 60 m*

### 4.2 Estimation of the texture autocorrelation sequence

To check the validity of the hypothesis made over the correlation times of the two components, we estimated the texture autocorrelation sequence with the formula

$$\hat{R}_\tau\left(\frac{Nm}{2}\right) = \frac{1}{N_b}\sum_{k=1}^{N_b-|m|}\hat{\tau}_k\hat{\tau}_{k+m} \quad (22)$$

and the texture covariance as

$$\hat{C}_\tau\left(\frac{Nm}{2}\right) = \frac{1}{N_b}\sum_{k=1}^{N_b-|m|}\hat{\tau}_k\hat{\tau}_{k+m} - \left[\frac{1}{N_b}\sum_{k=1}^{N_b}\hat{\tau}_k\right]^2 \quad (23)$$

It is useful to observe that with a 50% of overlap, we can estimate the texture correlation and covariance every $N/2$ lags. To estimate the texture correlation, we set $N = 128$. In the figures, we plot the texture correlation coefficient, that is

$$c_\tau\left(\frac{Nm}{2}\right) = \frac{\hat{C}_\tau(Nm/2)}{\hat{C}_\tau(0)} \quad (24)$$

Figs. 10–12 show the texture correlation coefficient. At the same resolutions and without differences in the polarisations, the texture correlation time is on the order of seconds. Furthermore, the texture presents periodicities with a period of 8 s at a range resolution of 60 m and of 3 s at a range resolution of 30 m. The periodicity is particularly evident in the
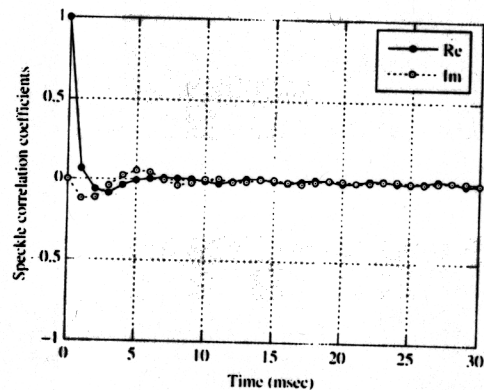


**Fig. 9** *Speckle correlation coefficients, VV polarisation, eighth cell, 3 m*
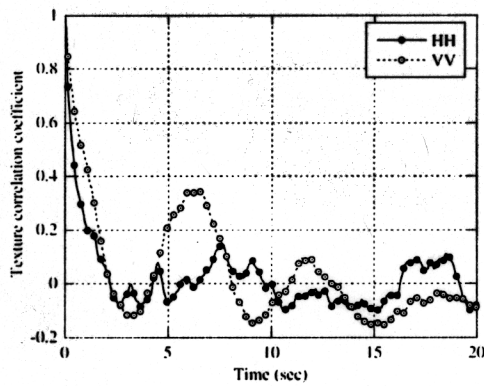
**Fig. 10** *Texture autocovariance function, first cell. N = 128, 60 m*

VV polarised data for the resolution of 60 m in all the files we analysed.

Our results show that, with increasing resolution, the texture correlation time decreases, but still in the order of a few seconds and the periodicities tend to disappear, due to the strong contribution of the thermal noise (Figs. 9 and 10).

Figs. 13 and 14 report an example of the average spectrogram in semi-logarithm scale for each considered cell, calculated as

$$P(k) = \frac{1}{N_{seq}} \sum_{r=1}^{N_{seq}} P_r(k) = \frac{1}{N_{seq}} \sum_{r=1}^{N_{seq}} \frac{1}{N_c} \left| \sum_{i=(r-1)N_c+1}^{rN_c} x(i) e^{-jkn} \right|^2,$$

$$k = 1, 2, \ldots, N_c \quad (25)$$

where $N_{seq}$ is the number of sequences in which the received vector for each cell has been divided, $N_c$ the number of samples per sequence, $k$ the normalised frequency and $P_r(k)$ is the $k$th sample of the periodogram of the $r$th sequence.

The periodogram shows, for all the polarisations, for all the range resolutions, a peak located around 150 Hz. Moreover, with a resolution of 60 and 30 m, all the analysed cells show a bimodal spectrum, particularly evident in HH polarisation, and then a second peak near −150 Hz; the power of the second peak is much lower than the power of the main one (Fig. 13). From the resolution of 15 m, the IPIX radar seems to add a frequency interfering line in the spectrum at about −220 Hz (Fig. 14). The line at
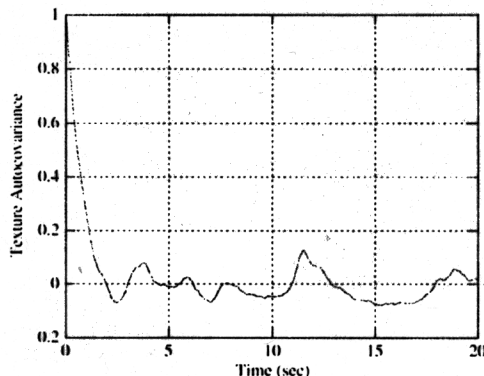


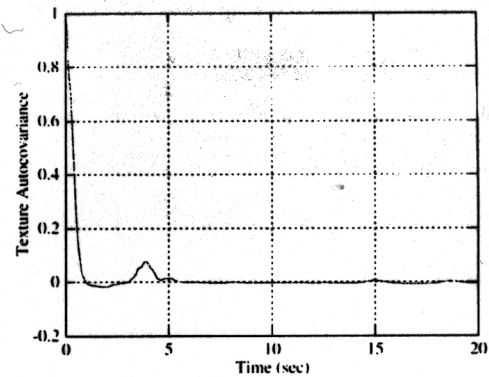**Fig. 11** *Texture autocovariance function, HH polarisation, first cell, 15 m*



**Fig. 12** *Texture autocovariance function, VV polarisation, eighth cell, 3 m*

0 Hz is due to a residual of the continuous component. It is evident that, as resolution increases, the thermal noise effect becomes very important. In fact, from our results, only partially shown here, it is evident that the clutter-to-noise ratio (CNR) decreases from ≃24 dB for a resolution of 60 m with VV data to less than −5 dB for a resolution of 3 m with VH data. The CNR has been roughly estimated from the spectrum figures reading the value of the noise floor from each figure and calculating clutter power as the difference between the overall
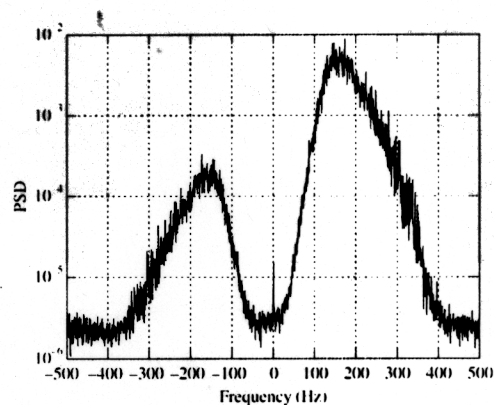


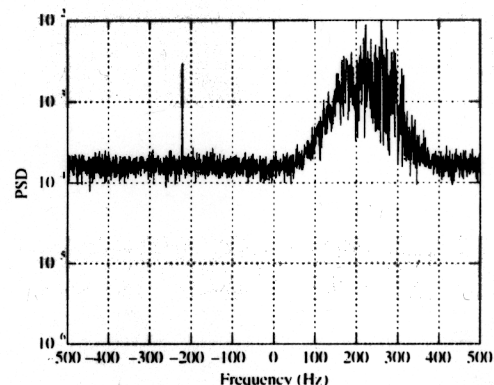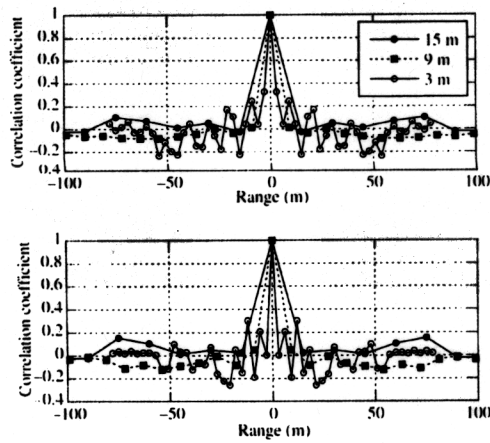**Fig. 13** *Average power spectral density, first cell, HH polarisation, 60 m, CNR ≃ 24 dB*



**Fig. 14** *Average power spectral density, VV polarisation, eighth cell, 3 m, CNR ≃ 4 dB*

**Fig. 15** *Mean range texture autocovariance, VV and HH polarisation*

disturbance power and noise power. The values calculated for each cell is reported in the figure captions.

### 4.3 Mean range texture autocovariance sequence

To conclude the correlation analysis, in order to highlight further differences due to the resolution, we also calculated the average range autocovariance function of the texture given by

$$\hat{R}_\tau(n) = \frac{1}{N_b} \sum_{m=1}^{N_b} \hat{R}_{\tau_m}(n)$$

$$= \frac{1}{N_b N_c} \sum_{m=1}^{N_b} \sum_{i=1}^{N_c-n} \left[\hat{\tau}_m(i) - \bar{\tau}_m\right]\left[\hat{\tau}_m(i+n) - \bar{\tau}_m\right] \quad (26)$$

where $\hat{\tau}_m(i)$ is the estimate of the texture on the $m$th burst of the $i$th cell, $N_c$ the number of illuminated cells, $N_b$ the number of bursts and $\bar{\tau}_m$ the texture average value in the $m$th burst

$$\bar{\tau}_m = \frac{1}{N_c} \sum_{i=1}^{N_c} \hat{\tau}_m(i) \quad (27)$$

Because at 30 m range resolution, the illuminated zone is different, we only compared the results found at 15, 9 and 3 m range resolutions.

Figs. 10 and 15 show the results obtained for VV and HH polarisations. From the figures it is evident that with a resolution of 3 m, it is possible to highlight and resolve shorter range periodicities that are not visible in the other resolutions in all the polarisations.

### 5 Conclusions

Our results, based on the analysis of many files at different range resolutions of the Grimsby data set, recorded by IPIX radar, reveal that the GK-PDF provides a good-fit to the data for all polarisations with resolutions of 60 and 30 m. Increasing the range resolution up to 15 m, the model consistently yields a good-fit in most cells for co-polarisations even if the presence of longer-tailed cells with respect to the lower resolutions has been observed. The model is valid for all VH–HV polarised data. At 9 and 3 m, both VV and HH polarisation histograms exhibit very long tails, so that the compound-Gaussian model is not valid any longer.

Moreover, at these resolutions, the thermal noise contribution becomes non-negligible. The GK model provides a good-fit in almost all cells for VH polarisation at 9 m, but at 3 m also the cross-polarisations present long-tailed cells and the compound model fails to provide a good-fit.

Estimated parameters analysis shows that HH component is the most spiky one at 60, 15, 9 and 3 m range resolution; at a resolution of 30 m, on average, an HH component is less spiky than both VV and VH components (remembering that at 30 m range resolution the illuminated zone is different).

Cumulants-domain analysis confirms the results obtained by the histograms analysis. At 9 m range resolution compound-Gaussian model provides a good-fit in most cells for VH polarisation. The fifth-order cumulant shows a large deviation from zero in most cells for both HH and VV polarisations.

At 3 m range resolution, most cells in all polarisations present estimated values of the cumulants very different from zero. In this instance, the deviation from the compound-Gaussian model is not due to the presence of thermal noise.

About the correlation and spectral analysis, based on our results, we can conclude that in all the analysed resolutions, in each polarisation, average speckle correlation time is ~10 ms. Moreover, without differences in the polarisations, the texture correlation time is some seconds long; the texture presents periodicities with a period of 8 s at a range resolution of 60 m and of 3 s at a range resolution of 30 m. The periodicity is particularly evident in the VV polarised data for the resolution of 60 m. With increasing resolution, the texture correlation time becomes shorter, but still on the order of a few seconds, and the periodicities tend to disappear, due to the strong contribution of the thermal noise. Differences in HH, VV and VH time covariances are not evident. Only in range, the VH texture exhibits a longer correlation time than the like-polarised data.

The analysis of the periodogram shows that for all the polarisations and all range resolutions, a peak is located around 150 Hz. Moreover, as the resolution increases, the thermal noise effect becomes very important; the *CNR* decreases from $\cong 24$ dB for a resolution of 60 m and VV data to less than $-5$ dB for a resolution of 3 m and VH data. Then, the presence of the thermal noise at very high resolution strongly affects the behaviour of the recorded disturbance.

### 6 Acknowledgments

### 7 References

1 Greco, M., and Gini, F.: 'Sea clutter non-stationarity: the influence of long-waves' in Simon H. (Ed.): 'Adaptive radar: toward the development of cognitive radar' (Wiley, 2006), Ch. 5, pp. 153–184
2 Currie, B.: 'Private communications', October 2003
3 Barnard, T.J., and Weiner, D.D.: 'Non-gaussian clutter modeling with generalized spherically invariant random vectors', *IEEE Trans. Signal Process.*, 1996, **44**, (10), pp. 2384–2390
4 Conte, E., and Longo, M.: 'Characterisation of radar clutter as a spherically invariant random process', *IEE Proc. F*, 1987, **134**, (2), pp. 191–197
5 Conte, E., De Maio, A., and Galdi, C.: 'Statistical analysis of real clutter at different range resolutions', *IEEE Trans. Aerosp. Electron. Syst.*, 2004, **40**, (3), pp. 903–918

6  Fay, F.A., Clarke, J., and Peters, R.S.: 'Weibull distribution applied to sea-clutter'. Proc. IEE Conf. on Radar '77, London, UK, 1977, pp. 101 103

7  Farina, A., Gini, F., Greco, M., and Verrazzani, L.: 'High resolution sea clutter data: a statistical analysis of recorded live data', *IEE Proc. F*, 1997, **144**, (3), pp. 121–130

8  Jakeman, E., and Pusey, P.N.: 'A model for non-Rayleigh sea echo'. *IEEE Trans. Antennas Propag.*, 1976, **AP-24**, pp. 806 814

9  Ward, K.D., Baker, C.J., and Watts, S.: 'Maritime surveillance radar. Part I: radar scattering from ocean surface', *IEE Proc. F*, 1990, **137**, (2), pp. 51 62

10  Rangaswamy, M., Weiner, D.D., and Ozturk, A.: 'Non-Gaussian vector identification using spherically invariant random processes', *IEEE Trans. Aerosp. Electron. Syst.*, 1993, **29**, (1), pp. 111–124

11  Rangaswamy, M., Weiner, D.D., and Ozturk, A.: 'Computer generation of correlated non-Gaussian radar clutter', *IEEE Trans. Aerosp. Electron. Syst.*, 1995, **31**, (1), pp. 106 115

12  Rangaswamy, M., Michels, J.H., and Weiner, D.D.: 'Multichannel detection algorithm for correlated non-Gaussian random processes based on innovations', *IEEE Trans. Signal Process.*, 1995, **43**, (8), pp. 1915 1922

13  Rangaswamy, M., and Michels, J.H.: 'A parametric multichannel detection for correlated non-Gaussian random processes'. Proc. National Radar Conference, Syracuse, NY, USA, May 1997, pp. 349–354

14  Rangaswamy, M., and Michels, J.H.: 'Adaptive signal processing in non-Gaussian noise backgrounds'. Proc. 9th IEEE-SSAP Workshop, Portland, OR, September 1998

15  Kay, S.M.: 'Fundamentals of statistical signal processing', Volume I, 'estimation theory' (Prentice-Hall, 1993)

16  Lehmann, E.L.: 'Testing statistical hypotheses' in 'Springer texts in statistics' (Springer, New York, 2nd edn.)

17  Gini, F.: 'A cumulant-based adaptive technique for coherent radar detection in a mixture of K-distributed clutter and Gaussian disturbance', *IEEE Trans. Signal Process.*, 1997, **45**, (6), pp. 1507–1519

18  Sadler, B., Giannakis, G.B., and Lii, K.S.: 'Estimation and detection in the presence of non-Gaussian noise', *IEEE Trans. Signal Process.*, 1994, **42**, (10), pp. 2729 2741

19  Gini, F., and Greco, M.: 'Texture modelling, estimation and validation using measured sea clutter data', *IEE Proc. Radar Sonar Navig.*, 2002, **149**, (3), pp. 115 124